

Lattice Schwinger Model and Spacetime Supersymmetry

Yanting Cheng^{1,2} and Shang Liu^{3,4,*}

¹*Institute of Theoretical Physics and Department of Physics,
University of Science and Technology Beijing, Beijing 100083, China*

²*Department of Physics and Hong Kong Institute of Quantum Science and Technology,
The University of Hong Kong, Pokfulam Road, Hong Kong SAR, China*

³*Kavli Institute for Theoretical Physics, University of California, Santa Barbara, California 93106, USA*

⁴*Department of Physics, California Institute of Technology, Pasadena, California 91125, USA*

Gauge theories in (1+1)D have attracted renewed attention partially due to their experimental realizations in quantum simulation platforms. In this work, we revisit the lattice massive Schwinger model and the (1+1)D lattice Abelian-Higgs model, uncovering previously overlooked universal features, including the emergence of a supersymmetric quantum critical point when the Maxwell term's coefficient changes sign. To facilitate the quantum simulation of these theories, we adopt a strategy of truncating the electric field eigenvalues to a finite subset, preserving the exact gauge and global symmetries. Our primary focus is the truncated lattice Schwinger model at $\theta = 0$, a model not equivalent to familiar spin models. We find that upon reversing the sign of the Maxwell term, the second-order deconfinement-confinement transition can become first-order, and the two types of transitions are connected by a supersymmetric critical point in the tricritical Ising universality class. In the case of truncated abelian-Higgs model at $\theta = 0$, which turns out to be equivalent to the quantum Blume-Capel model, the very existence of a deconfined phase requires a negative-sign Maxwell term. Similarly, there is a tricritical Ising point separating first-order and second-order phase transitions.

Introduction — Gauge theory stands as a cornerstone of modern theoretical physics, providing a mathematical framework to describe fundamental forces and emergent phenomena [1, 2]. Its principles play fundamental roles in the understanding of (de)confinement, quantum anomalies, and topological order in exotic quantum matter. Recently, the quantum simulation of gauge theories in one spatial dimension has emerged as a promising tool, offering a manageable setting for investigating complex dynamics and providing deeper insights into the fundamental laws of physics[3–26].

In (1+1)D, the simplest gauge theories with matter are the abelian-Higgs model and the (massive) Schwinger model, where the electromagnetic field is coupled to one flavor of complex boson field and one flavor of Dirac fermion field, respectively[27–32]. On top of the choices of matter field, there is also a parameter known as the topological angle θ which may be set to 0 or π ; other θ -angles are less interesting due to the absence of the charge conjugation symmetry and hence the absence distinct phases. Field theoretical properties of these four models can be found, for example, in Refs. 2 and 33.

In order to realize those gauge theories in quantum simulation platforms, it is preferable to have lattice versions of the models with finite-dimensional local Hilbert spaces. One common strategy towards this goal is to truncate the possible eigenvalues of electric field strength to a finite subset, in a way that preserves the exact gauge and global symmetries[34–36]. If we consider the truncated lattice models corresponding to the four gauge theories mentioned above, it turns out that three out of

the four models are equivalent to familiar spin models as summarized in Table I. Such equivalence can be established upon “integrating out” the matter degrees of freedom using the gauge redundancy: The case of Schwinger model at $\theta = \pi$ is discussed in Refs. 37–39, and the cases of abelian-Higgs model are explained in the Supplemental Material.

In this work, we focus on the remaining case, truncated lattice Schwinger model at $\theta = 0$, which is not equivalent to any familiar spin model. We determine the phase diagram and low-energy properties of this lattice model. Curiously, we go beyond the conventional parameter regime and allow the coefficient of Maxwell term (electric field energy term) to change sign, leading to surprisingly interesting results. When the coefficient is positive, there is a continuous deconfinement-confinement phase transition in the Ising universality class upon increasing the fermion mass. The same happens in the untruncated continuum version of the theory. When the coefficient is negative, it turns out that the deconfinement-confinement phase transition can become first-order and the two types of phase transition lines are connected by a tricritical point. The tricritical point is in the tricritical Ising universality class which is well-known to have emergent spacetime supersymmetry.

We note that similar interesting phenomena also occur in the truncated lattice abelian-Higgs model at $\theta = 0$. With a positive Maxwell term, the model is always in the confined phase and has no phase transition. However, a negative Maxwell term leads to a deconfined phase. The transition between these phases includes both a first-order part and an Ising-type second-order part, separated by a tricritical Ising point. These follow from known properties of the quantum Blume-Capel model as

* sliu.phys@gmail.com

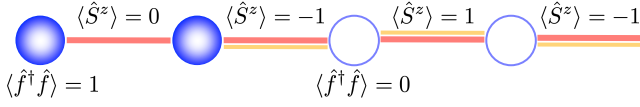


FIG. 1. A schematic diagram of a possible configuration. Fermions are placed on the sites, and gauge fields (spin-1) are on the links between sites.

explained in the Supplemental Material. We will not further discuss this model in the rest of the main text.

Model — The Kogut-Susskind Hamiltonian of the massive Schwinger model on a lattice is given by [40]

$$\hat{H} = \frac{1}{2a} \sum_n [\hat{f}_n^\dagger e^{i\hat{\phi}(n)} \hat{f}_{n+1} + h.c.] + m \sum_n (-1)^n \hat{f}_n^\dagger \hat{f}_n + \frac{1}{2} g^2 a \sum_n (\hat{L}(n) - \frac{\theta}{2\pi})^2, \quad (1)$$

where a is the lattice constant, g is the elementary charge, and m is the mass of the fermion. The operators \hat{f}_n^\dagger and \hat{f}_n represent the creation and the annihilation operator of a fermion on the site n , and the gauge field operators living on the link between site n and site $n+1$ obey the commutation relation

$$[\hat{\phi}(n), \hat{L}(l)] = i\delta_{n,l}, \quad (2)$$

which implies $[\hat{L}(n), e^{i\hat{\phi}(n)}] = e^{i\hat{\phi}(n)}$. The eigenvalues of $\hat{\phi}$ are defined modulo 2π , namely $\phi \sim \phi + 2\pi$. Accordingly, the eigenvalues of \hat{L} are integers \mathbb{Z} . The electric field strength is defined as $\hat{E}(n) = \hat{L}(n) - \frac{\theta}{2\pi}$, where θ angle is a background electric field. The Hamiltonian (1) is invariant under the local U(1) transformation that $\hat{f}_n \rightarrow \hat{f}_n e^{i\alpha}$, $e^{i\hat{\phi}(n-1)} \rightarrow e^{i(\hat{\phi}(n-1)-\alpha)}$ and $e^{i\hat{\phi}(n)} \rightarrow e^{i(\hat{\phi}(n)+\alpha)}$ for any particular n . Such gauge transformations are generated by the Gauss's law operator:

$$\hat{G}(n) = \hat{L}(n) - \hat{L}(n-1) - \hat{f}_n^\dagger \hat{f}_n + \frac{1}{2} [1 - (-1)^n]. \quad (3)$$

If not otherwise specified, we focus on the gauge invariant subspace defined by $\hat{G}(n) = 0$ for all n .

In the rest of this work, we only consider $\theta = 0$. The Hamiltonian (1) then exhibits the following charge conjugation symmetry:

$$\begin{aligned} \mathcal{C} e^{i\hat{\phi}(n)} \mathcal{C}^{-1} &= e^{-i\hat{\phi}(n+1)}, & \mathcal{C} \hat{E}(n) \mathcal{C}^{-1} &= -\hat{E}(n+1) \\ \mathcal{C} \hat{f}_n^\dagger \mathcal{C}^{-1} &= \hat{f}_{n+1}, & \mathcal{C} \hat{f}_n \mathcal{C}^{-1} &= \hat{f}_{n+1}^\dagger. \end{aligned} \quad (4)$$

If all low-energy states are nearly invariant under the action of \mathcal{C}^2 , we may expect \mathcal{C}^2 to approach the identity operator in the continuum limit, in which case the charge conjugation symmetry effectively becomes a \mathbb{Z}_2 symmetry.

From the perspective of experimental realization, it is preferable to have finite-dimensional local Hilbert spaces. This can be done by truncating the allowed eigenvalues of

the electric field $\hat{E}(n)$. We choose the simplest nontrivial truncation where $\hat{E}(n)$ can take values from 0 and ± 1 , implying the following substitution: $\hat{L}(n) \rightarrow \hat{S}_{n,n+1}^z$ and $e^{i\hat{\phi}(n)} \rightarrow \hat{S}_{n,n+1}^\pm / \sqrt{2}$. Moreover, we also implement the following transformations:

$$\begin{cases} \text{Odd } n : & f_n \rightarrow f_n^\dagger, f_n^\dagger \rightarrow f_n, \\ \text{Even } n : & \hat{S}_{n,n+1}^z \rightarrow -\hat{S}_{n,n+1}^z, \hat{S}_{n,n+1}^\pm \rightarrow \hat{S}_{n,n+1}^\mp. \end{cases} \quad (5)$$

which will help simply the charge conjugation symmetry. The resulting Hamiltonian is given by

$$\hat{H}_{\text{trunc}} = \frac{1}{2\sqrt{2}a} \sum_n [\hat{f}_n \hat{S}_{n,n+1}^+ \hat{f}_{n+1} + h.c.] + m \sum_n \hat{f}_n^\dagger \hat{f}_n + \frac{1}{2} g^2 a \sum_n (\hat{S}_{n,n+1}^z)^2. \quad (6)$$

This truncated lattice Schwinger model upholds an exact local U(1) gauge symmetry as well as a charge conjugation symmetry, similar to the original Schwinger model, although we truncated the values of the electric field. The Gauss's law operator is now given by

$$\hat{\hat{G}}(n) = (-1)^{n+1} (\hat{S}_{n,n+1}^z + \hat{S}_{n-1,n}^z + \hat{f}_n^\dagger \hat{f}_n). \quad (7)$$

Again, if not otherwise noted, we focus on the subspace where $\hat{\hat{G}}(n) = 0$. Within this subspace, the charge conjugation symmetry of \hat{H}_{trunc} is simply the translation symmetry, thanks to the transformations in Eq. 5. In terms of the truncated electric field $\hat{E}_{n,n+1} = (-1)^{n+1} \hat{S}_{n,n+1}^z$, we can rewrite the Gauss's law as $\hat{E}_{n,n+1} - \hat{E}_{n-1,n} = \hat{\hat{G}}(n) + (-1)^n \hat{f}_n^\dagger \hat{f}_n$. We will refer to $\hat{\hat{G}}(n)$ as the (non-dynamical) gauge charge and $(-1)^n \hat{f}_n^\dagger \hat{f}_n$ as the physical charge. Fig. 1 exemplifies a situation with no gauge charge present for the periodic boundary condition.

The gauge constraints indicate that the degrees of freedom associated with the matter field are entirely redundant. Especially, once the values of $\hat{S}_{n,n+1}^z$ for all links are known, the values of $\hat{f}_n^\dagger \hat{f}_n$ can be derived by Gauss's law. This observation implies that the model can be further simplified by “integrating out” the matter sites using the gauge redundancy. If $\hat{\hat{G}}(n) = 0$, the resulting Hamiltonian is

$$\hat{H}_{\text{spin-1}} = \sum_n \left[\frac{\sqrt{2}}{2a} \hat{S}_{n,n+1}^x - 2m \hat{S}_{n,n+1}^z + \frac{1}{2} g^2 a (\hat{S}_{n,n+1}^z)^2 \right], \quad (8)$$

under the constraint that $\hat{S}_{n,n+1}^z + \hat{S}_{n-1,n}^z = -\hat{f}_n^\dagger \hat{f}_n$ can only take eigenvalues 0 and -1 . Nonzero values of $\hat{\hat{G}}(n)$ will not affect the Hamiltonian up to an additive constant, but will modify the Hilbert space constraints as can be derived from (7). This equivalent formulation of the truncated Schwinger model obscures the gauge symmetry structure, but makes it easier to analyze the phase diagram.

	Abelian-Higgs model	Massive Schwinger Model
$\theta = 0$	Quantum Blume-Capel Model	<i>Spin-1 Model in This Work</i>
$\theta = \pi$	Quantum Ising Model	PXP Model

TABLE I. Equivalent spin models of truncated (1+1)D lattice gauge theories.

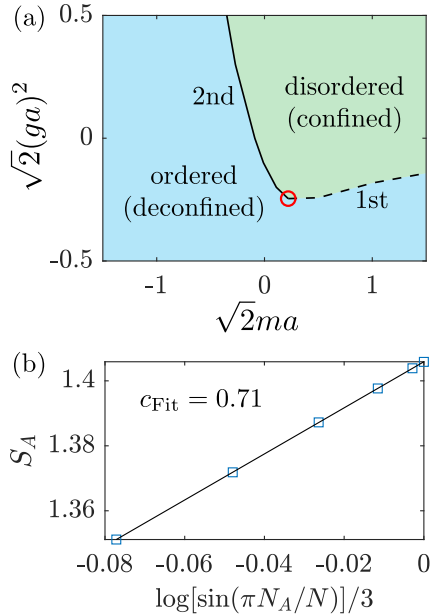


FIG. 2. (a) Phase diagram of the spin-1 massive lattice Schwinger model. A dashed line signifies the first-order phase transition and a solid line represents the second-order phase transition. The tricritical point, where these two lines intersect, is marked by a red circle. (b) Central charge at the tricritical point. By fitting the Calabrese-Cardy formula to the subsystem size N_A , the central charge at the tricritical point is obtained. These results come from the exact diagonalization of a 24-site system.

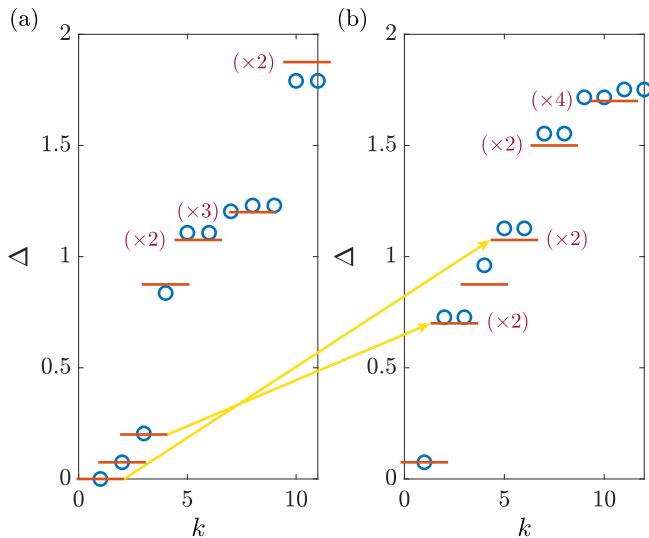


FIG. 3. Low energy spectrum for (a) $N = 28$ which corresponds to periodic boundary condition, and (b) $N = 27$ which corresponds to antiperiodic boundary condition.

Phase Diagram — Recall we focus on $\theta = 0$ where the Schwinger model has a global charge conjugation symmetry. In \hat{H}_{trunc} or $\hat{H}_{\text{spin-1}}$, this is nothing but the one-site translation symmetry. We denote the generator of this symmetry by \hat{M}_1 . For instance, $\hat{M}_1 \hat{A}_{n,n+1} \hat{M}_1^{-1} = \hat{A}_{n+1,n+2}$. One can check that when $\hat{G}(n) = 0$, \hat{M}_1 respects the gauge constraints and commutes with the Hamiltonian. We assume that in the continuum limit, this translation symmetry becomes an emergent \mathbb{Z}_2 symmetry, i.e. two-site translation acts trivially. Indeed, we have found no spontaneous breaking of the two-site translation symmetry in the parameter regime we explored, which is a necessary condition of the above assumption. In line with this emergent \mathbb{Z}_2 symmetry, we introduce the order parameter $\hat{O}_n = (-1)^n (\hat{S}_{n,n+1}^z - \hat{S}_{n-1,n}^z)$ to differentiate between the ordered and disordered phases as depicted in Fig. 2 (a). In the ordered phase where the \mathbb{Z}_2 symmetry is broken, $\lim_{r \rightarrow \infty} \langle \hat{O}_n \hat{O}_{n+r} \rangle \neq 0$. Conversely, in the disordered phase, $\lim_{r \rightarrow \infty} \langle \hat{O}_n \hat{O}_{n+r} \rangle = 0$.

As shown in the phase diagram Fig. 2 (a), both a first-order phase transition along the dashed line and a second-order phase transition along the solid line exist. When crossing the solid line from the ordered phase to the disordered phase, the two-point function gradually diminishes to zero. Conversely, when crossing the dashed line from the ordered phase to the disordered phase, the two-point function abruptly drops to zero. Another discriminating factor between the first-order and second-order phase transitions is the subsystem entanglement entropy. Notably, the entanglement entropy S_A along the solid line is significantly higher than that on either side of the solid line. In contrast, S_A along the dashed line does not exhibit a noticeable increase compared to that on both sides of the dashed line. By examining the dependence of S_A on the subsystem size N_A and fitting it to the Calabrese-Cardy formula [41] $S_A = c \log[\sin(\pi N_A/N)]/3 + S_0(N)$, we have found that the second-order transition line (except for its end point) is in the Ising universality class with central charge $c = 1/2$.

The first-order and second-order phase transition lines meet at a tricritical point marked by the red circle in the phase diagram. We anticipated that this tricritical point is in the tricritical Ising universality class with central charge $c = 7/10$, and thus determined its precise location, $\sqrt{2}(ma, g^2 a^2) = (0.224, -0.246)$ for $N = 24$, by maximizing the central charge fitted from entanglement entropy. See Fig. 2 (b) for the central charge fitting right at this tricritical point. The result is indeed closed to the expected theoretical value.

The conformal field theory describing the tricritical Ising point is known to have spacetime supersymmetry,

which imposes nontrivial relations between the energy spectra of periodic and antiperiodic boundary conditions (PBC and APBC). Therefore, let us compare the low-lying energy spectra of our lattice model with those predicted by the tricritical Ising conformal field theory. Note that in our lattice model, the Ising \mathbb{Z}_2 symmetry is realized as the translation symmetry, hence PBC and APBC should correspond to N being even and odd, respectively. In general, conformal symmetry in (1+1)D implies the energy eigenvalues E_k to take the following form:

$$E_k = \epsilon_0(N) + \frac{2\pi v}{Na} \Delta_k. \quad (9)$$

Here, $k = 1, 2, \dots$ labels the energy eigenstates, ϵ_0 is a system size dependent energy shift, v is the “speed of light”, and Δ_k are a set of universal numbers that depend on the specific conformal field theory and on the boundary condition. The set of Δ_k for the tricritical Ising theory with both PBC and APBC can be found, e.g. in Ref. 42. In Fig. 3, we have shown the comparison between the theoretical and numerical spectra. The two lowest states with $N = 28$ and one lowest state with $N = 27$ have been used to fix the three constants: $v, \epsilon_0(28), \epsilon_0(27)$. One can see that the remaining energy eigenvalues and degeneracies all fit reasonably well. As mentioned above, the spacetime supersymmetry relates PBC and APBC energy spectra. For example, a pair of superconformal symmetry generators (level $-1/2$) map the PBC state with $\Delta = 1/5$ to a pair of APBC states with $\Delta = 1/5 + 1/2 = 7/10$. Another pair of superconformal symmetry generators (level $-3/2$) map the PBC ground state with $\Delta = 0$ to a pair of APBC states with $\Delta = 0 + 3/2 = 3/2$. These and more other examples are all manifest in Fig. 3, confirming the emergence of supersymmetry.

Confinement-deconfinement transition — The spontaneous breaking of charge conjugation symmetry implies the deconfinement of charged particles and vice versa. We will first give a physical argument of this statement, and then numerically test it in our truncated lattice Schwinger model.

To facilitate our discussion, it is convenient to smear the notion of charge by defining $\hat{q}_{n,n+1} := (\hat{E}_{n+1,n+2} - \hat{E}_{n-1,n})/2$, which is the average charge over two neighboring sites n and $n+1$. Given the unbroken two-site translation symmetry, we have $\langle \hat{q}_{n,n+1} \rangle = 0$ in any vacuum state throughout the phase diagram. In the following, we will only consider such smeared charges if not otherwise specified. We say the system is in the deconfined (confined) phase if we are able (unable) to create isolated charges without costing extensive energy.

Suppose the charge conjugation symmetry is spontaneously broken. We must have at least two degenerate vacua [43] with nonzero and opposite order parameter values; they are related to each other by the action of \mathcal{C} . Note that the order parameter \hat{O}_n is actually proportional to the smeared electric field $(\hat{E}_{n-1,n} + \hat{E}_{n,n+1})/2$. Consequently, a domain wall between the two vacua car-

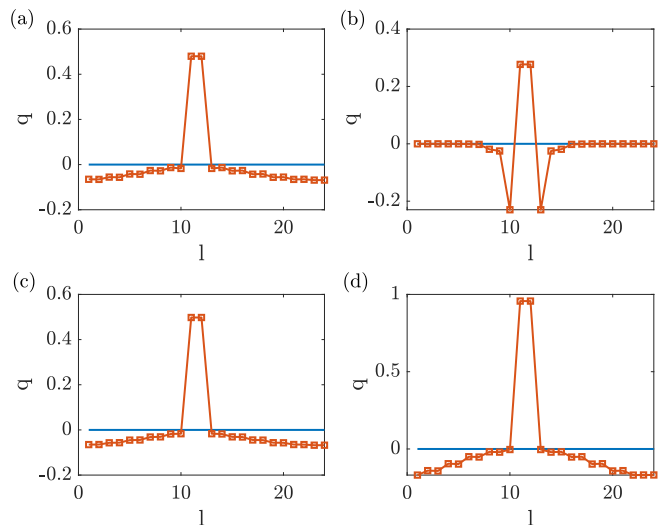


FIG. 4. The smeared charge distribution after adding gauge charges into the system for different phases. (a) $\sqrt{2}ma = -1$, $\sqrt{2}(ga)^2 = 0.5$. (b) $\sqrt{2}ma = 1$, $\sqrt{2}(ga)^2 = 0.5$. (c) $\sqrt{2}ma = -1$, $\sqrt{2}(ga)^2 = -0.5$. (d) $\sqrt{2}ma = 1$, $\sqrt{2}(ga)^2 = -0.5$

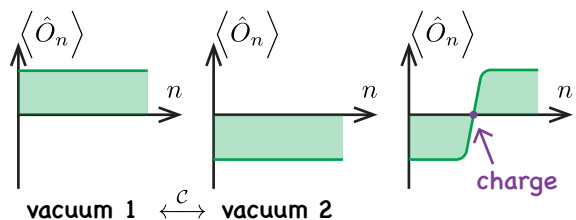


FIG. 5. A domain wall between degenerate vacua related by charge conjugation symmetry carries a nonzero charge.

ries a nonzero charge – proportional to the difference of order parameter values from the two vacua. See Fig. 5 for an illustration. Such a domain wall can be created by applying the charge conjugation on half of the space of one vacuum state. The existence of an unscreened charge with a localized energy density implies deconfinement. Conversely, if the system is in the deconfined phase, we should be able to create a pair of unscreened charges out of one vacuum and separate them apart, generating an energy density that is only nonzero near the charges. Now if we send the two charges all the way to spatial infinity, we have created a new vacuum state whose order parameter value differs from the original one. Therefore, at least one of the two vacua has a nonzero order parameter, implying the spontaneous breaking of the charge conjugation symmetry.

To numerically test whether a phase is confined or not, we introduce a localized gauge charge into the system and calculate the smeared charge distribution. If the additional charge is fully screened, the system is in the confinement phase. Otherwise, it is in the deconfinement phase. In Fig. 4, we introduce gauge charges into the

system with varying parameters m and g^2 , where we set

$$\hat{G}(n) = \begin{cases} 1 \text{ or } 2 & n = 12 \\ 0 & \text{otherwise.} \end{cases}$$

We then calculate the new ground state and the corresponding smeared charge distribution $\langle \hat{q}_{n,n+1} \rangle$, as shown in Fig. 4. For reference, the blue line represents the total charge distribution of the ground state under the condition that $\hat{G}(n) = 0$ for all n . In Fig. 4 (b), charges are localized around the additional gauge charge introduced, indicating that the system is in the confined phase. Conversely, in panels (a), (c), and (d), charges are delocalized, signifying that the system is in the deconfined phase. We note that in the case of Fig. 4 (d), while one unit of gauge charge appears to be fully screened, two units of gauge charges remain clearly unscreened, as shown in the figure.

Discussion — To summarize, we have discovered a supersymmetric quantum critical point – tricritical Ising point – in both the truncated lattice Schwinger model and the truncated (1+1)D abelian-Higgs model. Either case requires a negative-sign Maxwell term. An important theoretical question to explore is whether the aforementioned critical point exists in the untruncated or continuum versions of these models. It would be also interesting to find experimental realizations of the lattice Schwinger model studied here. Compared to another recent proposal for quantum simulating tricritical Ising point [44], our model makes it easier to realize antiperiodic boundary condition, but harder to realize an explicit fermion operator with a Jordan-Wigner string.

Acknowledgments — We thank Hui Zhai, Zhen-Sheng Yuan, Hanteng Wang and Ming-Gen He for the discussion. Y. C. is supported by NSFC Grant No. 12204034, No. 12374251, Fundamental Research Funds for the Central Universities (No.FRFTP22-101A1), HK CRF C4050-23GF, and C7012-21GF. S. L. acknowledges support from the Gordon and Betty Moore Foundation under Grant No. GBMF8690, the National Science Foundation under Grant No. NSF PHY-1748958, and the Simons Foundation under an award to Xie Chen (Award No. 828078).

SUPPLEMENTAL MATERIAL

Appendix A: Integrating Out Matter Field

1. Abelian-Higgs Model

The (1+1)D Abelian Higgs (AH) model can be defined on a 1D chain with sites labeled by $n \in \mathbb{Z}$ and links labeled by $(n, n+1)$. The physical degrees of freedom on each site (link) may be regarded as a particle moving on a ring with the periodic boundary condition (some twisted boundary condition). On a site, we have

$$[\hat{\varphi}, \hat{p}] = i, \quad \varphi \sim \varphi + 2\pi, \quad p \in \mathbb{Z}. \quad (\text{S1})$$

It follows that $e^{i\hat{\varphi}}(\hat{p} + 1) = \hat{p}e^{i\hat{\varphi}}$, which means the effect of $e^{i\hat{\varphi}}$ is to increase p by 1. On a link, we have

$$[\hat{a}, \hat{E}] = i, \quad a \sim a + 2\pi, \quad E \in \mathbb{Z} - \frac{\theta}{2\pi}, \quad (\text{S2})$$

where the parameter θ should be identical for all links. Similarly, $e^{i\hat{a}}$ increases E by 1. The AH model has the following Hamiltonian.

$$\hat{H}_{\text{AH}} = \sum_n (-J e^{i\hat{\varphi}_n} e^{i\hat{a}_{n,n+1}} e^{-i\hat{\varphi}_{n+1}} + h.c.) + \frac{1}{2}\mu \sum_n \hat{p}_n^2 + \frac{1}{2}g^2 \sum_i \hat{E}_{n,n+1}^2. \quad (\text{S3})$$

In addition, the following Gauss' law is imposed on the Hilbert space

$$\hat{G}_n := \hat{E}_{n,n+1} - \hat{E}_{n-1,n} - \hat{p}_n = 0. \quad (\text{S4})$$

Notice that \hat{G}_n commutes with \hat{H}_{AH} , thus the physical subspace defined above is an invariant subspace of \hat{H}_{AH} . We assume $J \geq 0$ without loss of generality and also $\mu \geq 0$. The first two terms are obtained by minimally coupling the O(2) rotor model [45] to the U(1) gauge field and the last term is the Maxwell term (gauge field kinetic energy). We expect that in some continuum limit, this lattice model should describe a complex boson field ϕ coupled with electromagnetic field. Large μ/J should correspond to large positive boson mass, while $\mu/J \rightarrow 0$ corresponds to large negative boson mass. However, we did not attempt to carefully derive the continuum limit, thus our convention for the coupling constants is somewhat arbitrary.

The gauge constraint (S4) implies that the matter field degrees of freedom are completely redundant. Indeed, once we know the values of $E_{n,n+1}$ for all n , we can derive the values of all p_n using the Gauss' law. This observation formally means the following isomorphism of Hilbert spaces.

$$\begin{aligned} (\text{sites} \otimes \text{links})|_{\hat{G}_n=0 \forall n} &\rightarrow \text{links} \\ |\{p_n\}, \{E_{n,n+1}\}\rangle &\mapsto |\{E_{n,n+1}\}\rangle \end{aligned} \quad (\text{S5})$$

It is not hard to check that the above explicit mapping is indeed one-to-one. It follows that we can ‘‘integrate out’’ all the matter field[46]. The effective Hamiltonian thus obtained is

$$\begin{aligned} \hat{H}_{\text{eff}} &= \sum_n (-J e^{i\hat{a}_{n,n+1}} + h.c.) + \frac{1}{2}\mu \sum_i (\hat{E}_{n,n+1} - \hat{E}_{n-1,n})^2 + \frac{1}{2}g^2 \sum_i \hat{E}_{n,n+1}^2 \\ &= \sum_n (-J e^{i\hat{a}_{n,n+1}} + h.c.) - \mu \sum_i \hat{E}_{n-1,n} \hat{E}_{n,n+1} + \left(\frac{1}{2}g^2 + \mu\right) \sum_i \hat{E}_{n,n+1}^2. \end{aligned} \quad (\text{S6})$$

a. Truncated Model at $\theta = \pi$

Now consider $\theta = \pi$ and we truncate the electric field space to only retain $E = \pm 1/2$. We can then substitute

$$\hat{E} \mapsto \begin{pmatrix} 1/2 & 0 \\ 0 & -1/2 \end{pmatrix}, \quad e^{i\hat{a}} \mapsto \begin{pmatrix} 0 & 1 \\ 0 & 0 \end{pmatrix}. \quad (\text{S7})$$

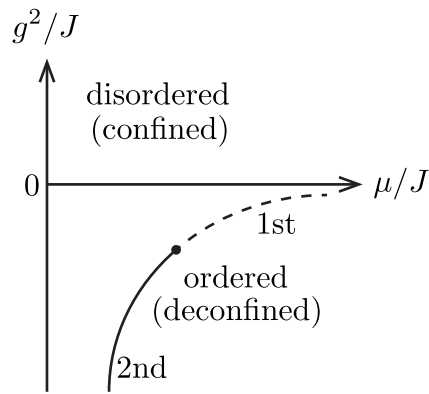


FIG. S1. Schematic phase diagram of the truncated lattice AH model at $\theta = 0$.

These substitutions preserve the $U(1)$ gauge symmetry generated by G_n as well as the global charge conjugation symmetry $(\hat{E}, \hat{a}, \hat{p}, \hat{\varphi}) \mapsto -(\hat{E}, \hat{a}, \hat{p}, \hat{\varphi})$. The procedure of integrating out matter fields works in the same way, and the effective Hamiltonian becomes

$$\hat{H}_{\text{eff}} \mapsto -J \sum_i \hat{X}_{i+1/2} - \frac{1}{4} \mu \sum_i \hat{Z}_{i-1/2} \hat{Z}_{i+1/2}, \quad (\text{S8})$$

which is exactly the transverse field Ising model. The ordered (disordered) phase of the Ising model corresponds to the deconfined (confined) phase of the AH model.

b. Truncated Model at $\theta = 0$

At $\theta = 0$, we may truncate the model to by retaining $E = 0, \pm 1$, or equivalently applying the substitutions

$$\hat{E} \mapsto \begin{pmatrix} 1 & 0 & 0 \\ 0 & 0 & 0 \\ 0 & 0 & -1 \end{pmatrix}, \quad e^{i\hat{a}} \mapsto \begin{pmatrix} 0 & 1 & 0 \\ 0 & 0 & 1 \\ 0 & 0 & 0 \end{pmatrix}. \quad (\text{S9})$$

Using spin-1 operators, the resulting effective Hamiltonian is

$$H_{\text{eff}} \mapsto -\sqrt{2}J \sum_n \hat{S}_{n,n+1}^x - \mu \sum_i \hat{S}_{n-1,n}^z \hat{S}_{n,n+1}^z + \left(\frac{1}{2}g^2 + \mu \right) \sum_i (\hat{S}_{n,n+1}^z)^2. \quad (\text{S10})$$

This is the quantum Blume-Capel model [47]. The schematic phase diagram looks like Fig. S1; see Refs. 47 and 48 for details. Note that there is no confinement-deconfinement transition when the Maxwell term is positive, which is consistent with the result of the continuum AH model [2].

2. Schwinger Model

For (truncated) lattice Schwinger models, such as the $\theta = 0$ model studied in the main text, the procedure of integrating out matter sites is similar but slightly more tricky. There are two caveats: (1) The fermion number $\hat{f}_n^\dagger \hat{f}_n$ can only be 0 or 1, which leads to residue constraints on the spins after integrating out matters. (2) We need to be careful about the ordering of fermion operators.

Let us elaborate this procedure for the model considered in the main text. We fix the values of $\hat{G}(n)$, say all zero, and let $\mathcal{L}_{\text{sites+links}}$ be the Hilbert space for both sites and links under the Gauss's law constraints. \hat{H}_{trunc} acts within this Hilbert space. As we mentioned in the main text, the Gauss's law implies that all site variables are actually redundant. More precisely, we expect $\mathcal{L}_{\text{sites+links}}$ to be isomorphic to another Hilbert space $\mathcal{L}_{\text{links}}$ which only consists of the spins on the links and is subject to the following constraints: $(-1)^{n+1} \hat{G}(n) - \hat{S}_{n,n+1}^z - \hat{S}_{n-1,n}^z$ can only take

eigenvalues 0 and 1. Let $\hat{\nu}_n := \hat{f}_n^\dagger \hat{f}_n$. We can explicitly write down an isomorphism $\mathcal{L}_{\text{sites+links}} \rightarrow \mathcal{L}_{\text{links}}$ as follows:

$$|\{\nu_n\}, \{S_{n,n+1}^z\}\rangle := (\hat{f}_N^\dagger)^{\nu_N} (\hat{f}_{N-1}^\dagger)^{\nu_{N-1}} \dots (\hat{f}_1^\dagger)^{\nu_1} |\{S_{n,n+1}^z\}\rangle \mapsto |\{S_{n,n+1}^z\}\rangle. \quad (\text{S11})$$

One can check that under this isomorphism, we have the following operator mapping rules:

$$\begin{cases} \hat{f}_n \hat{S}_{n,n+1}^+ \hat{f}_{n+1} \mapsto \hat{\mathcal{P}} \hat{S}_{n,n+1}^+ \hat{\mathcal{P}} & 1 \leq n \leq N-1 \\ \hat{f}_N \hat{S}_{N,1}^+ \hat{f}_1 \mapsto (-1)^{\nu_N + \nu_{N-1} + \dots + \nu_1 - 1} \hat{\mathcal{P}} \hat{S}_{N,1}^+ \hat{\mathcal{P}} & n = N \end{cases}, \quad (\text{S12})$$

where $\hat{\mathcal{P}}$ is the projection operator onto the allowed spin configurations. The sign factor in the second line is actually a constant depending on the values of $\hat{G}(n)$:

$$\sum_n \nu_n = \sum_n (-1)^{n+1} \hat{G}(n) \pmod{2}. \quad (\text{S13})$$

The mapping rules for other operators in the Hamiltonian is rather obvious, for example,

$$\hat{f}_n^\dagger \hat{f}_n \mapsto (-1)^{n+1} \hat{G}(n) - \hat{S}_{n,n+1}^z - \hat{S}_{n-1,n}^z. \quad (\text{S14})$$

The extra sign factor mentioned above is rather annoying, but we can actually remove it by applying a local spin rotation generated by $\hat{S}_{N,1}^z$. Such a rotation commutes with $\hat{S}_{n,n+1}^z$ and thus preserves both the spin configuration constraints and other terms in the Hamiltonian. Finally, we obtain the equivalent Hamiltonian $\hat{H}_{\text{spin-1}}$ given in the main text.

The case of $\theta = \pi$ works in a similar way and the result can be found in Refs. 37–39.

- [1] A. M. Polyakov, *Gauge Fields and Strings* (Taylor & Francis, 1987).
- [2] D. Tong, Gauge theory, Lecture notes, DAMTP Cambridge **10**, 8 (2018).
- [3] H. P. Büchler, M. Hermele, S. D. Huber, M. P. A. Fisher, and P. Zoller, Atomic Quantum Simulator for Lattice Gauge Theories and Ring Exchange Models, *Phys. Rev. Lett.* **95**, 040402 (2005).
- [4] T. Byrnes and Y. Yamamoto, Simulating lattice gauge theories on a quantum computer, *Phys. Rev. A* **73**, 022328 (2006).
- [5] E. Zohar, J. I. Cirac, and B. Reznik, Simulating Compact Quantum Electrodynamics with Ultracold Atoms: Probing Confinement and Nonperturbative Effects, *Phys. Rev. Lett.* **109**, 125302 (2012).
- [6] D. Banerjee, M. Dalmonte, M. Müller, E. Rico, P. Stebler, U.-J. Wiese, and P. Zoller, Atomic Quantum Simulation of Dynamical Gauge Fields Coupled to Fermionic Matter: From String Breaking to Evolution after a Quench, *Phys. Rev. Lett.* **109**, 175302 (2012).
- [7] U.-J. Wiese, Ultracold quantum gases and lattice systems: quantum simulation of lattice gauge theories, *Annalen der Physik* **525**, 777 (2013).
- [8] P. Hauke, D. Marcos, M. Dalmonte, and P. Zoller, Quantum Simulation of a Lattice Schwinger Model in a Chain of Trapped Ions, *Phys. Rev. X* **3**, 041018 (2013).
- [9] E. Rico, T. Pichler, M. Dalmonte, P. Zoller, and S. Montangero, Tensor Networks for Lattice Gauge Theories and Atomic Quantum Simulation, *Phys. Rev. Lett.* **112**, 201601 (2014).
- [10] T. Pichler, M. Dalmonte, E. Rico, P. Zoller, and S. Montangero, Real-Time Dynamics in U(1) Lattice Gauge Theories with Tensor Networks, *Phys. Rev. X* **6**, 011023 (2016).
- [11] E. A. Martinez, C. A. Muschik, P. Schindler, D. Nigg, A. Erhard, M. Heyl, P. Hauke, M. Dalmonte, T. Monz, P. Zoller, and R. Blatt, Real-time dynamics of lattice gauge theories with a few-qubit quantum computer, *Nature* **534**, 516 (2016).
- [12] N. Klco, E. F. Dumitrescu, A. J. McCaskey, T. D. Morris, R. C. Pooser, M. Sanz, E. Solano, P. Lougovski, and M. J. Savage, Quantum-classical computation of schwinger model dynamics using quantum computers, *Phys. Rev. A* **98**, 032331 (2018).
- [13] C. Kokail, C. Maier, R. van Bijnen, T. Brydges, M. K. Joshi, P. Jurcevic, C. A. Muschik, P. Silvi, R. Blatt, C. F. Roos, and P. Zoller, Self-verifying variational quantum simulation of lattice models, *Nature* **569**, 355 (2019).
- [14] F. M. Surace, P. P. Mazza, G. Giudici, A. Lerose, A. Gambassi, and M. Dalmonte, Lattice Gauge Theories and String Dynamics in Rydberg Atom Quantum Simulators, *Phys. Rev. X* **10**, 021041 (2020).
- [15] B. Yang, H. Sun, R. Ott, H.-Y. Wang, T. V. Zache, J. C. Halimeh, Z.-S. Yuan, P. Hauke, and J.-W. Pan, Observation of gauge invariance in a 71-site Bose–Hubbard quantum simulator, *Nature* **587**, 392 (2020).
- [16] A. Mil, T. V. Zache, A. Hegde, A. Xia, R. P. Bhatt, M. K. Oberthaler, P. Hauke, J. Berges, and F. Jendrzejewski, A scalable realization of local u(1) gauge invariance in cold atomic mixtures, *Science* **367**, 1128 (2020).

- [17] Z.-Y. Zhou, G.-X. Su, J. C. Halimeh, R. Ott, H. Sun, P. Hauke, B. Yang, Z.-S. Yuan, J. Berges, and J.-W. Pan, Thermalization dynamics of a gauge theory on a quantum simulator, *Science* **377**, 311 (2022).
- [18] Z.-Y. Zhou, G.-X. Su, J. C. Halimeh, R. Ott, H. Sun, P. Hauke, B. Yang, Z.-S. Yuan, J. Berges, and J.-W. Pan, Thermalization dynamics of a gauge theory on a quantum simulator, *Science* **377**, 311 (2022).
- [19] N. H. Nguyen, M. C. Tran, Y. Zhu, A. M. Green, C. H. Alderete, Z. Davoudi, and N. M. Linke, Digital quantum simulation of the schwinger model and symmetry protection with trapped ions, *PRX Quantum* **3**, 020324 (2022).
- [20] N. Mueller, J. A. Carolan, A. Connelly, Z. Davoudi, E. F. Dumitrescu, and K. Yeter-Aydeniz, Quantum computation of dynamical quantum phase transitions and entanglement tomography in a lattice gauge theory, *PRX Quantum* **4**, 030323 (2023).
- [21] D. Pomarico, L. Cosmai, P. Facchi, C. Lupo, S. Pascasio, and F. V. Pepe, Dynamical quantum phase transitions of the schwinger model: Real-time dynamics on ibm quantum, *Entropy* **25**, 10.3390/e25040608 (2023).
- [22] H.-Y. Wang, W.-Y. Zhang, Z. Yao, Y. Liu, Z.-H. Zhu, Y.-G. Zheng, X.-K. Wang, H. Zhai, Z.-S. Yuan, and J.-W. Pan, Interrelated thermalization and quantum criticality in a lattice gauge simulator, *Phys. Rev. Lett.* **131**, 050401 (2023).
- [23] W.-Y. Zhang, Y. Liu, Y. Cheng, M.-G. He, H.-Y. Wang, T.-Y. Wang, Z.-H. Zhu, G.-X. Su, Z.-Y. Zhou, Y.-G. Zheng, H. Sun, B. Yang, P. Hauke, W. Zheng, J. C. Halimeh, Z.-S. Yuan, and J.-W. Pan, Observation of microscopic confinement dynamics by a tunable topological θ -angle, *Nature Physics* [10.1038/s41567-024-02702-x](https://doi.org/10.1038/s41567-024-02702-x) (2024).
- [24] C. Charles, E. J. Gustafson, E. Hardt, F. Herren, N. Hogan, H. Lamm, S. Starecheski, R. S. Van de Water, and M. L. Wagman, Simulating F_2 lattice gauge theory on a quantum computer, *Phys. Rev. E* **109**, 015307 (2024).
- [25] R. C. Farrell, M. Illa, A. N. Ciavarella, and M. J. Savage, Scalable circuits for preparing ground states on digital quantum computers: The schwinger model vacuum on 100 qubits, *PRX Quantum* **5**, 020315 (2024).
- [26] J. Mildenerger, W. Mruczkiewicz, J. C. Halimeh, Z. Jiang, and P. Hauke, Confinement in a \mathbb{Z}_2 lattice gauge theory on a quantum computer, *Nature Physics* [10.1038/s41567-024-02723-6](https://doi.org/10.1038/s41567-024-02723-6) (2025).
- [27] P. W. Anderson, Plasmons, gauge invariance, and mass, *Phys. Rev.* **130**, 439 (1963).
- [28] F. Englert and R. Brout, Broken symmetry and the mass of gauge vector mesons, *Phys. Rev. Lett.* **13**, 321 (1964).
- [29] P. W. Higgs, Broken symmetries and the masses of gauge bosons, *Phys. Rev. Lett.* **13**, 508 (1964).
- [30] G. S. Guralnik, C. R. Hagen, and T. W. B. Kibble, Global conservation laws and massless particles, *Phys. Rev. Lett.* **13**, 585 (1964).
- [31] J. Schwinger, Gauge Invariance and Mass, *Phys. Rev.* **125**, 397 (1962).
- [32] J. Schwinger, Gauge Invariance and Mass. II, *Phys. Rev.* **128**, 2425 (1962).
- [33] R. Dempsey, I. R. Klebanov, S. S. Pufu, and B. Zan, Discrete chiral symmetry and mass shift in the lattice Hamiltonian approach to the Schwinger model, *Physical Review Research* **4**, 043133 (2022).
- [34] D. Horn, Finite matrix models with continuous local gauge invariance, *Physics Letters B* **100**, 149 (1981).
- [35] P. Orland and D. Rohrlich, Lattice gauge magnets: Local isospin from spin, *Nuclear Physics B* **338**, 647 (1990).
- [36] S. Chandrasekharan and U.-J. Wiese, Quantum link models: A discrete approach to gauge theories, *Nuclear Physics B* **492**, 455 (1997).
- [37] F. M. Surace, P. P. Mazza, G. Giudici, A. Lerosé, A. Gambassi, and M. Dalmonte, Lattice gauge theories and string dynamics in rydberg atom quantum simulators, *Phys. Rev. X* **10**, 021041 (2020).
- [38] Y. Cheng, S. Liu, W. Zheng, P. Zhang, and H. Zhai, Tunable Confinement-Deconfinement Transition in an Ultracold-Atom Quantum Simulator, *PRX Quantum* **3**, 040317 (2022).
- [39] Y. Cheng and H. Zhai, Emergent $u(1)$ lattice gauge theory in rydberg atom arrays, *Nature Reviews Physics* **6**, 566 (2024).
- [40] J. Kogut and L. Susskind, Hamiltonian formulation of wilson's lattice gauge theories, *Phys. Rev. D* **11**, 395 (1975).
- [41] P. Calabrese and J. Cardy, Entanglement entropy and conformal field theory, *Journal of Physics A Mathematical General* **42**, 504005 (2009).
- [42] Y. Zou and G. Vidal, Emergence of conformal symmetry in quantum spin chains: Antiperiodic boundary conditions and supersymmetry, *Phys. Rev. B* **101**, 045132 (2020).
- [43] The term “vacua” refers to ground states satisfying the cluster decomposition property.
- [44] C. Li, S. Liu, H. Wang, W. Zhang, Z.-X. Li, H. Zhai, and Y. Gu, Uncovering Emergent Spacetime Supersymmetry with Rydberg Atom Arrays, *Phys. Rev. Lett.* **133**, 223401 (2024).
- [45] S. Sachdev, *Quantum phase transitions* (Cambridge University Press, 2011).
- [46] Although we say “integrate out”, no physical degree of freedom is ignored during this process.
- [47] F. C. Alcaraz, J. R. Drugowich de Felício, R. Köberle, and J. F. Stilck, Hamiltonian studies of the Blume-Emery-Griffiths model, *Phys. Rev. B* **32**, 7469 (1985).
- [48] J. C. Xavier and F. C. Alcaraz, Precise determination of quantum critical points by the violation of the entropic area law, *Phys. Rev. B* **84**, 094410 (2011).